short communications

Metal sites in 3,4-dihydroxy-2-butanone 4-phosphate synthase from *Methanococcus jannaschii* in complex with the substrate ribulose 5-phosphate

Stefan Steinbacher,[a]*‡ **Susanne Schiffmann,**[b] **Adelbert Bacher**[b] **and Markus Fischer**[b]

[a]Max-Planck-Institut für Biochemie, Abteilung für Strukturforschung, Am Klopferspitz 18a, D-82152 Martinsried, Germany, and [b]Technische Universität München, Lehrstuhl für Organische Chemie und Biochemie, Lichtenbergstrasse 4, D-85747 Garching, Germany

‡ Present address: California Institute of Technology, Division of Chemistry and Chemical Engineering, Pasadena, CA 91125, USA.

Correspondence e-mail: steinbac@caltech.edu

The crystal structure of *Methanococcus jannaschii* 3,4-dihydroxy-2-butanone 4-phosphate synthase in complex with the substrate ribulose 5-phosphate at a dimetal centre has recently been determined at 1.7 Å resolution. The enzyme converts ribulose 5-phosphate into 3,4-dihydroxy-2-butanone 4-phosphate, while its C4 atom is released as formate. The resulting four-carbon body supplies all eight C atoms for the xylene moiety of riboflavin. Three of the four hydroxyl groups of ribulose 5-phosphate were coordinated by the metal ions. Based on crystallographic refinement, the metals were assigned as zinc and calcium, which were present in the crystallization buffer. Neither metal supports the enzymatic reaction. In the present study, the correctness of this assignment is assessed using anomalous diffraction data collected at the high-energy side of the zinc absorption edge ($\lambda = 1.2823$ Å). Only the three tentative zinc ions give strong peaks in an anomalous difference Fourier map ($>20\sigma$), whereas the four tentative calcium ions do not show anomalous signals above the noise level. These results confirm the initial assignment. In addition, the resolution was improved to 1.55 Å.

1. Intoduction

Riboflavin (vitamin B_2) is biosynthesized in numerous microorganisms and plants but not in animals, which depend on nutritional sources. Its derivatives, flavin mononucleotide (FMN) and flavinadenine dinucleotide (FAD), are indispensable in all cells, where they serve in a variety of redox reactions (Müller, 1992).

3,4-Dihydroxy-2-butanone 4-phosphate synthase (DHBPS) supplies the building blocks for the assembly of the xylene ring of the vitamin (Volk & Bacher, 1988). In fact, all eight C atoms of the xylene moiety are derived from the product of the enzyme. In the biosynthetic pathway, 3,4-dihydroxy-2-butanone 4-phosphate is condensed with 5-amino-6-ribitylamino-2,4(1*H*,3*H*)-pyrimidinedione derived from GTP (Scheuring *et al.*, 2001; Volk & Bacher, 1988). The reaction product, 6,7-dimethyl-8-ribityllumazine, undergoes a highly unusual dismutation catalyzed by riboflavin synthase which involves the exchange of a four-carbon fragment between two identical substrate molecules. The dismutation yields riboflavin and 5-amino-6-ribitylamino-2,4(1*H*,3*H*)-pyrimidinedione, which is recycled as substrate of 6,7-dimethyl-8-ribityllumazine synthase (Plaut, 1960).

The reaction catalyzed by DHBPS involves the release of C atom 4 of the substrate, ribulose 5-hosphate, as formate (Volk & Bacher, 1988, 1991). Moreover, the 1-hydroxy group of the substrate is removed. The overall reaction yields a 1-deoxytetrulose phosphate from the pentulose phosphate substrate (Ru5P). Mechanistic studies suggest that the reaction is initiated by the formation of an enediol, which resembles a postulated intermediate of ribulose bisphosphate carboxylase (Rubisco; Peach *et al.*, 1978; Pierce *et al.*, 1986).

The structure of *Escherichia coli* DHBPS has been determined by X-ray crystallography (Liao *et al.*, 2001) and by NMR spectroscopy (Kelly *et al.*, 2001). A fortuitous complex of the enzyme from *M. grisea* with glycerol used as cryoprotectant helped to define the active site (Liao *et al.*, 2002). Recently, we determined the crystal structure of DHBPS from the archaebacterium *Methanococcus jannaschii* in complex with the substrate ribulose 5-phosphate and divalent metals (Steinbacher *et al.*, 2003). Based on crystallographic refinement and the nature of the metal ligands, we assigned the metals at the active site to be zinc and calcium. Anomalous diffraction data collected at the high-energy side of the zinc absorption edge ($\lambda = 1.2823$ Å) now affirm that this assignment was correct.

2. Experimental

Crystals of the *M. jannaschii* DHBPS mutant His147Ser were grown as described in Steinbacher *et al.* (2003). The substrate complex was prepared by soaking a crystal with 2 m*M* ribulose 5-phosphate for 1 h. The crystal used

in this study is not identical to that of the previously described substrate complex.

X-ray data were collected at 100 K under cryogenic conditions using an Oxford Cryostream on a MAR Research 345 image-plate detector at beamline BW6 at DESY in Hamburg at $\lambda = 1.2823$ Å. Diffraction intensities were integrated and reduced using the *HKL* suite (Otwinowski & Minor, 1997) and the *CCP*4 suite (Collaborative Computational Project, Number 4, 1994).

The starting coordinates were those of the essentially isomorphous *M. jannaschii* DHBPS crystal structure refined at 1.7 Å (Steinbacher *et al.*, 2003). Refinement steps consisting of conjugate-gradient minimization, simulated annealing and *B*-factor refinement were carried out with the program *CNS* using the mlf target (Brünger *et al.*, 1998). For cross-validation, a random test set of 5% of the total number of reflections was excluded from the refinement and used for calculation of the free *R* factor (Brünger, 1992). Non-crystallographic symmetry restraints were not applied during the refinement. The Ramachandran plot (Ramachandran & Sasisekharan, 1968) calculated with the program *PROCHECK* (Laskowski *et al.*, 1993) showed no residues with angular values in forbidden areas.

3. Results and discussion

3.1. Data collection and refinement

The point mutant His147Ser of *M. jannaschii* DHBPS, which showed only ~10% of the wild-type enzymatic activity, yielded a monoclinic crystal form as described previously (Steinbacher *et al.*, 2003). This crystal form with a dimer in the asymmetric unit (Fig. 1) could be soaked with the substrate ribulose 5-phosphate in a
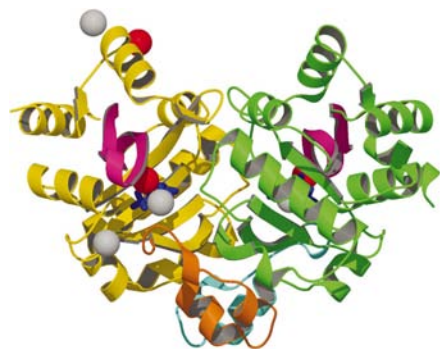
Table 1
Data collection.

Values in parentheses are for the last resolution shell.

Wavelength (Å)	1.2823
Limiting resolution (Å)	20–1.55 (1.59–1.55)
Space group	$P2_1$
Unit-cell parameters (Å, °)	$a = 53.4$, $b = 69.4$, $c = 57.6$, $\beta = 93.6$
R_{merge}† (%)	4.4 (26.7)
Unique reflections	53846
Completeness	88.3 (92.8)
Bijvoet pairs measured	38244
Anomalous completeness	62.7 (62.6)
$I/\sigma(I)$	17.5 (2.0)
Multiplicity	2.4

† $R_{merge} = \sum_{hkl}[(\sum_i |I_i - \langle I \rangle|)/\sum_i I_i]$.

suitable cryoprotectant in the presence of zinc and calcium ions. Regardless of the presence of substrate, metal I (zinc) is bound to His164. Binding of metal II (calcium) requires binding of the substrate (Fig. 2). For the present study, diffraction data were collected at the absorption edge of zinc at a wavelength of 1.2823 Å to a resolution of 1.55 Å (Table 1) to discriminate both potential divalent metals.

The structure was refined to a crystallographic *R* factor of 20.0% ($R_{free} = 23.4\%$). The resulting temperature factors of the metals are in agreement with their assignment as zinc and calcium (Table 2). The structure is essentially identical to that solved and refined at 1.7 Å. It shows ordered residues Asn2–Tyr220 and Asn3–Leu221 for the two asymmetric monomers and 347 solvent molecules. In addition, each active site contained one molecule of ribulose 5-phosphate and two metal ions, presumably zinc and calcium from the crystallization buffer, bound at the active site, with each metal ion binding an additional water ligand. The average temperature factors of Ru5P (22.9 Å^2) and metal ions at the active site

Table 2
Refinement statistics.

Resolution range (Å)	20–1.55
Reflections (working set)	51097 (83.9%)
Reflections (test set)	2723 (4.5%)
R_{cryst}† (%)	20.0
R_{free}‡ (%)	23.4
Non-H protein atoms	3472
Solvent molecules	352
B factors (Å^2)	
Protein	24.0
Solvent	32.8
Active-site metals	Zn, 18.9, 21.8;
(monomers *A* and *B*)	Ca, 20.3, 28.5
Other metals	Zn, 17.9;
	Ca, 24.7, 20.6
Ru5P (monomers *A* and *B*)	22.1, 23.7
R.m.s.d.	
Bond length (Å)	0.0105
Bond angle (°)	1.48

† $R_{cryst} = \sum_{hkl \subset W} ||F_{obs}| - k|F_{calc}||/\sum_{hkl \subset W} |F_{obs}|$. ‡ $R_{free} = \sum_{hkl \subset T} ||F_{obs}| - k|F_{calc}||/\sum_{hkl \subset T} |F_{obs}|$.

(22.4 Å^2) were slightly lower than for the protein (24.0 Å^2), which indicates full occupancy and a high degree of ordering. The Tyr95 loop is observed in two conformations. The acidic active-site loop from Tyr20 to Asp30 was well ordered in both monomers.

3.2. Active-site architecture and metal-mediated binding of ribulose 5-phosphate

We have observed two metal ions at the active site of *M. jannaschii* DHBPS, which we have identified as Zn^{2+} (metal I) and Ca^{2+} (metal II) (Steinbacher *et al.*, 2003). This assignment was based on the crystallographic refinement of temperature factors at 1.7 Å resolution, which should allow discrimination between both options assuming full occupancy (Ca, 20 electrons; Zn, 30 electrons). An anomalous difference Fourier map calculated with data collected at the

Figure 1
Ribbon diagram of the *M. jannaschii* DHBPS (Steinbacher *et al.*, 2003) dimer. Calcium and zinc ions are shown as grey and red balls, respectively. The bound substrate Ru5P is depicted as a blue ball-and-stick model and the acidic loop is in purple.
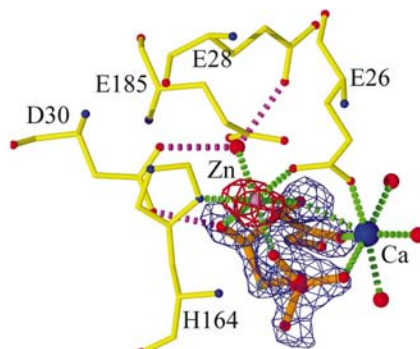

Figure 2
Active-site architecture. Metal-mediated binding mode of the substrate ribulose 5-phosphate (monomer *B*). The $2F_o - F_c$ density for Ru5P is shown at a 1.5σ contour level in blue. An anomalous difference Fourier map with data collected at the zinc absorption edge ($\lambda = 1.2823$ Å) is shown at a 15σ contour level in red. Metal I is clearly identified as zinc. The absence of an anomalous signal at metal II rules out zinc, which leaves calcium as a candidate for metal II.

high-energy side of the zinc absorption edge (λ = 1.2823 Å) shows three strong peaks of 32.5, 30.0 and 22.9σ, which are well above the noise level ($<8\sigma$). As calculated with the program *CROSSEC* (Collaborative Computational Project, Number 4, 1994), at this wavelength about 3.9 anomalous electrons are expected for zinc compared with 0.92 for calcium. The strong peaks are associated with metal I at both active sites of the asymmetric dimer (Fig. 2) and the metal involved in crystal packing, which were previously assigned as zinc ions. Only very weak density is observed at or close to the calcium ions.

The phosphate moiety of the substrate ribulose 5-phosphate is anchored by four hydrogen bonds (side chain and backbone amide of Thr165, backbone amide of His164) and four salt-bridge interactions (Arg25 and Arg161). In addition, each of the two metal ions is coordinated by a phosphate O atom (Fig. 2). The carbohydrate chain of ribulose 5-phosphate is fixed by four metal coordination bonds, two of which are formed by zinc (metal I) to O3 and O4 and two by calcium (metal II) to O2 and O3. Only one direct protein–substrate interaction is observed, between O4 and the side chain of Asp30 from the acidic loop. The O1 hydroxyl group appears in two conformations and has a somewhat weaker electron density which can be explained by the lack of direct contacts. Both metal ions show one water ligand in addition to the protein and substrate contacts. A prominent water molecule is found near O3 that is coordinated by Glu28 of the acidic loop and Glu185.

3.3. Other divalent metal-binding sites

A well defined zinc ion bridges $N^{\delta 1}$ of His206 of one dimer to a crystallographically related dimer which contributes Glu128 as a monodentate and Glu132 as a bidentate ligand. In addition, two calcium ions are found on the outer surface of the protein in monomer *A*. One calcium ion is bound by Asp96 and Glu97, and the second by the backbone carbonyl of Glu204 and the side chain of Asn207. In both cases, water molecules complete the coordination shells. The second calcium ion is only 9.0 Å from the zinc ion mediating a crystal lattice contact. Interestingly, neither calcium-binding site is occupied in monomer *B* as the ligands are involved in crystal-packing interactions. Asn207 forms a hydrogen bond with Asp61 of a neighbouring molecule, whereas Asp96 packs against the backbone amide of Asn136 and Glu97 forms a salt bridge with Lys65. These observations suggest that the binding sites have only a low affinity for calcium and are very likely to be of no physiological relevance.

It should be mentioned that the zinc-binding sites have one histidine side chain each as a ligand, whereas the calcium ions have none. For the active-site metals the different binding properties may reflect different roles during catalysis. Metal I defines the compact geometry of C3–C5 which is required for the migration of C5 to C3 during skeletal rearrangement. Metal II appears to make essential contributions to the initial 2,3-enediol formation and to the elimination of 1-OH as water. The temperature factor of metal II is also significantly higher in monomer *B* (28.5 Å^2) compared with monomer *A* (20.3 Å^2), which indicates a weaker binding. The coordination sphere of metal II is more variable as Tyr95 is a ligand only in monomer *A*. This flexibility may support conformational changes during the reaction.

References

Brünger, A. (1992). *Nature (London)*, **355**, 472–475.

Brünger, A. T., Adams, P. D., Clore, G. M., DeLano, W. L., Gros, P., Grosse-Kunstleve, R. W., Jiang, J.-S., Kuszewski, J., Nilges, M., Pannu, N. S., Read, R. J., Rice, L. M., Simonson, T. & Warren, G. L. (1998). *Acta Cryst.* D**54**, 905–921.

Collaborative Computational Project, Number 4 (1994). *Acta Cryst.* D**50**, 760–763.

Kelly, M. J., Ball, L. J., Krieger, C., Yu, Y., Fischer, M., Schiffmann, S., Schmieder, P., Kuhne, R., Bermel, W., Bacher, A., Richter, G. & Oschkinat, H. (2001). *Proc. Natl Acad. Sci. USA*, **98**, 13025–13030.

Laskowski, R. A., MacArthur, M. W., Moss, D. S. & Thornton, J. M. (1993). *J. Appl. Cryst.* **26**, 283–291.

Liao, D.-I., Calabrese, J. C., Wawrzak, Z., Viitanen, P. V. & Jordan, D. B. (2001). *Structure*, **9**, 11–18.

Liao, D.-I., Zheng, Y.-J., Viitanen, P. V. & Jordan, D. B. (2002). *Biochemistry*, **41**, 1795–1806.

Müller, F. (1992). Editor. *Chemistry and Biochemistry of Flavoenzymes.* Boca Raton, FL, USA: CRC Press.

Otwinowski, Z. & Minor, W. (1997). *Methods Enzymol.* **276**, 307–326.

Peach, C., Pierce, J., McCurry, S. D. & Tolbert, N. (1978). *Biochem. Biophys. Res. Commun.* **83**, 1084–1092.

Pierce, J., Andrews, T. J. & Lorimer, G. (1986). *J. Biol. Chem.* **261**, 10248–10256.

Plaut, G. W. E. (1960). *J. Biol. Chem.* **235**, 41–42.

Ramachandran, G. N. & Sasisekharan, V. (1968). *Adv. Protein. Chem.* **23**, 283–437.

Scheuring, J., Kugelbrey, K., Weinkauf, S., Cushman, M., Bacher, A. & Fischer, M. (2001). *J. Org. Chem.* **66**, 3811–3819.

Steinbacher, S., Schiffmann, S., Richter, G., Huber, R., Bacher, A. & Fischer, M. (2003). *J. Biol. Chem.* **278**, 42256–42265.

Volk, R. & Bacher, A. (1988). *J. Am. Chem. Soc.* **110**, 3651–3653.

Volk, R. & Bacher, A. (1991). *J. Biol. Chem.* **266**, 20610–20618.